# (9-Isocyanoanthracene)gold(I) Complexes Exhibiting Two Modes of Crystal Jumps by Different Structure Change Mechanisms

Kenta Kato,[a,b] Tomohiro Seki,[a,c,*] Hajime Ito[a,b,*]

[a] Division of Applied Chemistry & Frontier Chemistry Center, Faculty of Engineering, Hokkaido University, Sapporo, Hokkaido 060-8628, Japan.

[b] Institute for Chemical Reaction Design and Discovery (WPI-ICReDD), Hokkaido University 001-0021, Japan.

[c] Department of Chemistry, Faculty of Science, Shizuoka University, 836 Ohya, Suruga-ku, Shizuoka 422-8529, Japan.

Email: seki.tomohiro@shizuoka.ac.jp; hajito@eng.hokudai.ac.jp

**ABSTRACT:** The first examples of single crystals exhibiting salient effects by different structure change mechanisms are reported. The crystals of newly prepared aryl(9-isocyanoanthracene)gold(I) complexes jump in response to two different external stimuli: ultraviolet (UV) irradiation and cooling. The photosalient effect is triggered by photodimerization reaction of the anthracene moieties under photoirradiation. By contrast, the thermosalient effect is caused by anisotropic thermal contraction upon cooling without chemical structure change. By taking advantage of the multiple jump feature, we also show sequential jumps of crystals by cooling and then UV irradiation for demonstration of programmed motion of molecular crystals.

## INTRODUCTION

Crystal jumping phenomena, so-called salient effects of organic crystals, have been known for a long time,[1] and they were first reported in 1983.[2] Typically, photoirradiation and thermal treatment initiate salient effects, which are accordingly called the photosalient effect (Scheme S1) and thermosalient effect (Scheme S2), respectively (Figure 1a). In the last decade, salient effects have attracted considerable attention in terms of their mechanisms and possible application to microactuators or sensors.[1a,c] Photosalient effects are mostly triggered by photochemical covalent/coordination bond formation, such as ring-opening/closing reactions,[3] cycloadditions,[4] rearrangement,[5] and linkage isomerization,[6] upon photoirradiation. The molecular structure changes by these covalent/coordination bond formations result in accumulation of lattice strain in the crystal. The strain is then released in a short time, resulting in the crystal jumping.[7] Thermosalient effects are caused by a packing structure change with[2,8–42] or without[43] a thermal phase transition upon temperature change. This structural alternation generates strain within the crystal. The release of this accumulated strain then results in the crystal jumping. Salient-active crystals are known to show common crystallographic features during salient phenomena. They exhibit the same space group, a small cell volume change, and an anisotropic lattice dimension change before and after jumping.[1b]

Salient crystals that can jump by multiple mechanisms with different types of stimulation are attractive for designing micractuators with programmed motions.[1c] However, creation of a crystal that exhibits two different jumping modes by different mechanisms is difficult because of the complexity of salient phenomena. In fact, a single crystal exhibiting salient effects caused by two different mechanisms has not been reported. Naumov's group reported that a single crystal of (phenylazophenyl)palladium hexafluoroacetylacetonate, which exhibits the thermosalient effect in the crystalline form,[2a,8] can also jump upon photoirradiation after incubation of the compound in a polymer film.[44] The same group also reported that thermosalient crystals of terephthalic acid jump upon mechanical stimuli by the same phase transition as the structure change for the thermosalient effect.[45] However, there is no clear example of a single crystal with multiple structure change mechanisms for jumping. Development of a "multisalient" crystal remains a challenge in the crystal engineering field.

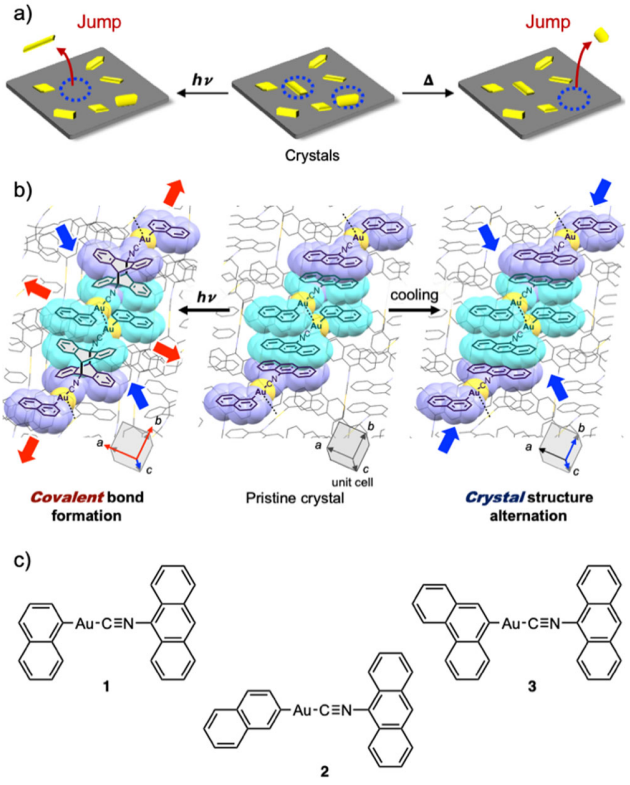


**Figure 1.** (a) Schematic image of salient effects. (b) Schematic representation of the two mechanisms of the photosalient effect and thermosalient effect of **1**. The red and blue arrows schematically indicate expansion and shrinking of the unit cell dimensions, respectively. (c) Molecular structures of **1**, **2**, and **3**.

Herein, we report newly synthesized aryl(9-isocyanoanthracene)gold(I) complexes (**1**, **2**, and **3**) exhibiting both the photosalient effect and thermosalient effect based on different mechanisms (Figures 1b, 1c and Figure S1). Single-crystal X-ray diffraction (XRD) analysis indicated that the photosalient effect was triggered by photodimerization of the anthracene skeletons under photoirradiation. By contrast, temperature-dependent XRD analysis indicated that the thermosalient effect of these complexes was initiated by anisotropic thermal contraction without chemical structure change upon cooling. The mechanism difference of these salient effects enabled a crystalline sample to sequentially exhibit both salient effects. These complexes are the first examples exhibiting two different salient effects in a single crystal.

## RESULTS AND DISCUSSION

The gold(I) isocyanide complexes with the 9-isocyanoanthracene ligand (1, 2, and 3) were synthesized by a similar procedure to that described in our previous report.46 Reactions of the chloro(9-isocyanoanthracene)gold(I) complexes and the corresponding organozinc reagents at 0 °C for 15 min afforded 1, 2, and 3 in good yield (89%–99%). The structures of 1, 2, and 3 were confirmed by 1H NMR spectroscopy and high-resolution mass spectrometry (HRMS).

The crystalline samples of **1**, **2**, and **3** exhibited both the photosalient effect and thermosalient effect. Crystalline samples were prepared by recrystallization, for example, a solution of **1** in $CHCl_3$ was slowly evaporated in the dark to give yellow crystals after a few days. The crystals remained intact at room temperature in the dark. However, upon UV irradiation at 365 nm, the crystals of **1** rapidly fragmented after moving (Figures 2a, S2a and Movie S1). Almost all of the samples of **1** exhibited the photosalient effect. Irradiation with longer wavelength light (405 and 435 nm) also resulted in the photosalient effect (Figures S2b, S2c and Movies S2, S3). Remarkably, a temperature change also induced the thermosalient effect. When crystals of **1** were cooled on a cooling plate at 50 °C/min, the crystals also jumped (Figures 2b, S3 and Movie S4). The temperature at which the crystals jumped was different in each experiment, ranging from −90 to −110 °C. This could be because of the rapid cooling speed and different crystal size/quality, as commonly observed for crystals exhibiting the thermosalient effect.[38] Compared with the photosalient effect of **1**, the probability of the thermosalient effect was not high (approximately 5% of the crystals jumped). The different jumping probabilities of the photosalient effect and thermosalient effect of **1** would indicate the existence of different mechanisms. Crystals of **2** and **3** were prepared by a similar method to that for preparation of crystals of **1**. The crystals of **2** and **3** also exhibited the photosalient effect (Figures S4, S5 and Movies S5–S10) and thermosalient effect (Figures S6 and Movies S11, S12).

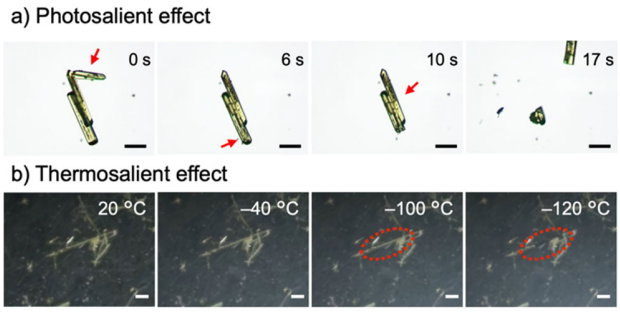


**Figure 2.** (a) Photographs showing the photosalient effect of **1** under UV light (365 nm). The red arrows indicate the crystal that jumps by the photosalient effect. Scale bars represent 50 mm. (b) Photographs showing the thermosalient effect of **1** upon cooling at 50 °C/min. The red ellipses indicate the crystal that jumps by the thermosalient effect. Scale bars represent 200 mm.

To investigate the mechanisms of both salient effects of **1**, single-crystal XRD analysis of an as-prepared single crystal of **1** was first performed at 20 °C. Complex **1** was found to crystallize in the monoclinic $P2_1/n$ space group (Table S1), with all of the molecules being crystallographically equivalent (Figure S7). The **1** molecules in the crystal adopt a planar conformation with a small dihedral angle between the naphthalene and anthracene rings [$\theta$ = 5.1(3)°, Figure S8]. The **1** molecules in

the planar conformation constitute a π-stacked dimer in a head-to-tail orientation (Figure 3a). This π-stacked dimer forms Au(I)···Au(I) and π–π interactions. The Au(I)···Au(I) distance is 3.6714(5) Å. The displaced π–π distances between the naphthyl and anthryl moieties are 3.410 Å. This π–π stacking slips with a parallel displacement of 1.577 Å (Figure S9).[47] These π-stacked dimers of **1** further form CH/π and π–π interactions between their anthracene moieties and neighboring π-stacked dimers (Figure 3b). The CH/π distance between the hydrogen atom in the anthryl group and the carbon atom in the naphthyl group is 2.862 Å. The π–π distance between the anthryl groups of neighboring π-stacked dimers is 3.616 Å. The anthryl groups are stacked with a parallel displacement of 1.453 Å (Figure S9).[47] As a result, **1** forms a herringbone structure within the (101) plane (Figure 3b). Upon UV irradiation, photodimerization of the anthryl groups proceeds at the C9 and C10 carbon atoms between the π-stacked dimers.[48] Between the π-stacked dimers, the reactive carbon–carbon distance in the anthracene moiety (C9–C10′ and C9′–C10) is 3.891 Å (Figure 3c). This carbon–carbon distance is within the limit of 4.2 Å proposed by Schmidt for photodimerization.[49] This information indicates that the anthracene moiety of **1** has structural potential to allow photodimerization in the crystalline state.

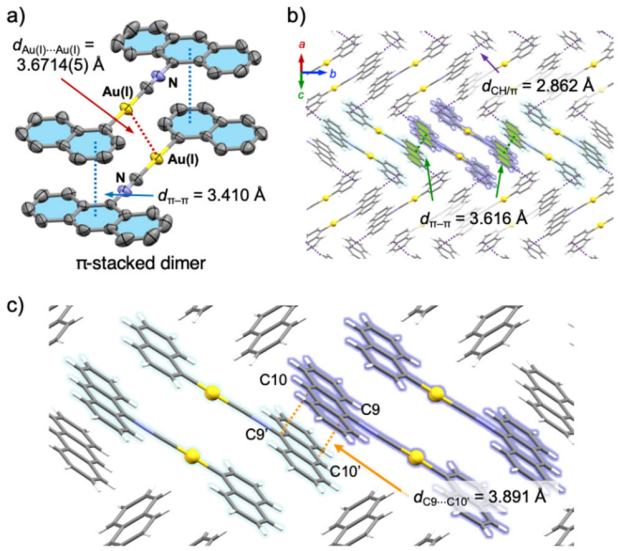


**Figure 3.** (a) ORTEP drawing of the π-stacked dimer of **1** at 20 °C. Hydrogen atoms are omitted for clarity. (b) Herringbone structure of **1** within the (101) plane. Three π-stacked dimers are highlighted in cyan or purple. (c) Distance between the reactive carbon atoms (C9–C10′ and C9′–C10) of **1**. Two adjacent π-stacked dimers are highlighted in cyan and purple.

Single-crystal XRD analysis of a photoirradiated single crystal of **1** was performed to reveal the mechanism of its photosalient effect. The fragmented crystals obtained after photoirradiation in air were too small and not suitable for single-crystal XRD analysis. When single crystals of **1** in Paratone oil were exposed to sunlight for a week, photoreacted single crystals suitable for XRD analysis were obtained. The crystal color of **1** changed from yellow to colorless by photodimerization (Figure 4a). Single-crystal XRD analysis of the colorless crystal was then performed at 20 °C, showing formation of the photodimer **1**$_{PD}$, in which the C9 and C10′ atoms are connected through newly formed covalent bonds (Figures 4b and S10).[50–52] In the single crystal of **1**$_{PD}$, the photodimer **1**$_{PD}$ is packed in the monoclinic space group $P2_1/n$, which is the same space group as before photoirradiation (Table S1). The asymmetric unit contains one half of the molecular structure of **1**$_{PD}$. **1**$_{PD}$ forms Au(I)···Au(I) interactions of 3.463(1) Å,[53] which are shorter than those in pristine **1**, constructing the herringbone structure (Figure 4c). A single crystal of **1**$_{PD}$ could not be prepared from $CHCl_3$ solution of **1**$_{PD}$ because **1**$_{PD}$ was unstable and easily decomposed in the solution state.

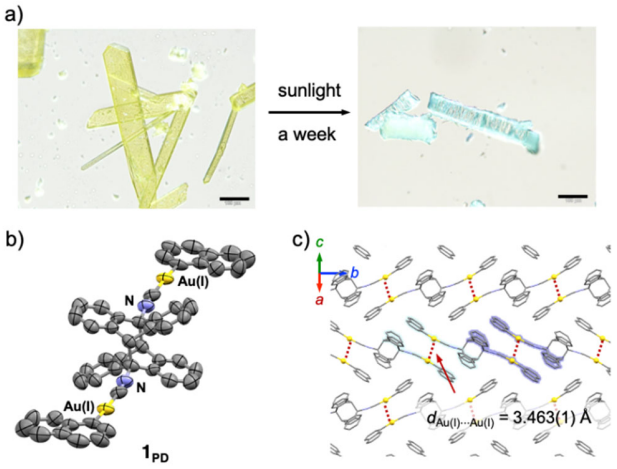


**Figure 4.** (a) Images of single crystals of **1** before and after sunlight irradiation in Paratone oil. The scale bar is 100 μm. (b) ORTEP drawing of the molecular structure of **1**$_{PD}$. Hydrogen atoms are omitted for clarity. (c) Packing structure of **1**$_{PD}$. The moieties of **1**$_{PD}$ highlighted in cyan and purple are originally included in two different pairs of π-stacked dimers of **1**.

Next, the crystal structures of **1** and **1**$_{PD}$ are compared to understand the crystal structure change upon photoirradiation (Figure 5a). As often observed in previous examples of photosalient compounds, the crystal structures of **1** and **1**$_{PD}$ are similar. Upon photodimerization from **1** to **1**$_{PD}$, the space group (monoclinic $P2_1/n$) is retained and the change of the unit cell volume is small ($\Delta V$ = +16.84 Å$^3$, +0.9%).[54] The crystal packing overlay of **1** and **1**$_{PD}$ viewed along the *a* axis provides a visual understanding of the anisotropic lattice change as a result of photodimerization (Figure 5b). Upon photodimerization, the length of the *c* axis decreases by about 5.0%, while the lengths of the *a* and *b* axes increase by about 2.9% and 3.7%, respectively. This anisotropic lattice dimension change is the origin of the photosalient effect of **1**.

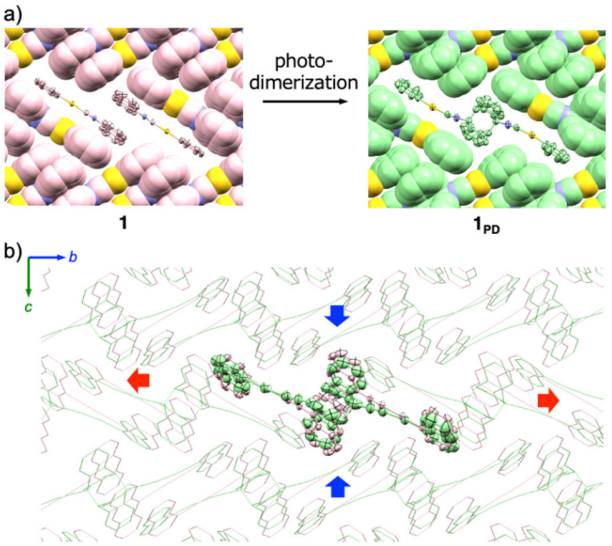


**Figure 5.** (a) Packing structures of **1** and **1**$_{PD}$ represented by the ORTEP and space-filling model. The carbon atoms of **1** and **1**$_{PD}$ are shown in pink and light green, respectively. Hydrogen atoms are omitted for clarity. (b) An overlay image of the packing structures of **1** and **1**$_{PD}$ viewed along the *a* axis. The crystallographic axes *b* and *c* are indicated by arrows. The red and blue arrows indicate the directions of expansion and shrinking of the packing structure by photodimerization along the *b* and *c* axes, respectively.

We then investigated the structure change of **1** upon the thermosalient effect. Temperature-dependent single-crystal XRD analysis of **1** revealed that the thermosalient effect of **1** was caused by anisotropic thermal contraction without a phase change upon cooling. We performed single-crystal XRD analysis of **1** from 20 to −140 °C with a 20 °C interval. The crystal qualities were all satisfactory for XRD analysis (Figure S13), and the results are summarized in Table S1. All of the crystal structures at different temperatures were similar, that is, they had the same space group (monoclinic $P2_1/n$) with only a small change of the unit cell volume ($\Delta V$ = −36.17 (−1.9%); 20 °C → −140 °C) (Figure 6a). In the π-stacked dimer, the Au(I)···Au(I) distance decreased from 3.6714(5) to 3.6124(5) Å upon cooling. The lattice dimensions of **1** slightly and anisotropically changed upon cooling. The lengths of the crystallographic *b* and *c* axes slightly decreased upon cooling ($\Delta b$ = −0.058 Å (−0.5%); $\Delta c$ = −0.210 Å (−1.5%); 20 °C → −140 °C), while that of the *a* axis remained almost the same [$\Delta a$ = +0.003 Å (+0.0%)]. A crystal packing overlay of **1** at 20 and −140 °C viewed along the *b* axis provides a visual understanding of the anisotropic crystal lattice change upon cooling (Figure 6b). Focusing on the **1** molecules, we found that the molecules keep their positions along the direction of the *a* axis upon cooling (20 → −140 °C), while they slightly approached each other along the *c* axis (blue arrows in Figure 6b). These results are consistent with the aforementioned anisotropic changes in the lengths of the crystallographic axes upon cooling ($\Delta a \approx 0$; $\Delta c < 0$).[55,56] This anisotropic lattice dimension change would be the origin of the thermosalient effect of **1**. From temperature-dependent single-crystal XRD and differential scanning calorimetry (DSC) analyses of **1**, we found that the crystal of **1** did not show the thermal phase transition upon the thermosalient effect.[57] We plotted the lengths of the *a*, *b*, and *c* axes of **1** against temperature and found the absence of an abrupt change (Figure S16). These structures and thermal measurements indicate that the thermosalient effect of **1** does not occur through a thermoinduced phase transition. Moreover, DSC analysis of **1** from −140 to 100 °C gave a featureless trace, indicating the absence of a thermal phase transition during this salient effect (Figure S17). The absence of a phase transition during the thermosalient effect has been reported, but it is rare.[43]

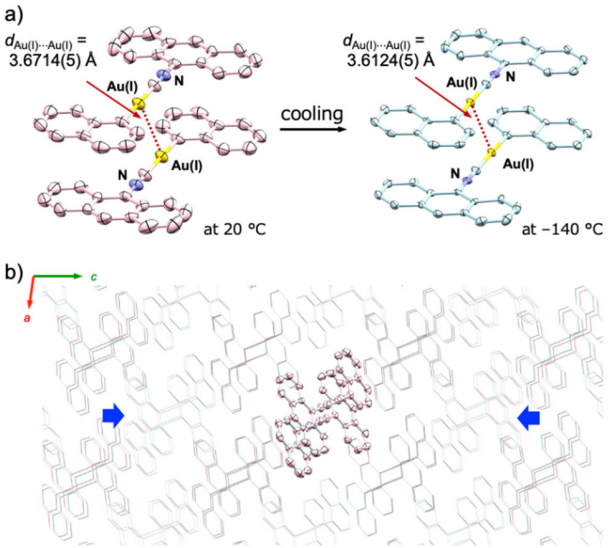


**Figure 6.** (a) ORTEP drawings of the π-stacked dimers of **1** at 20 and −140 °C. The carbon atoms at 20 and −140 °C are shown in pink and light blue, respectively. Hydrogen atoms are omitted for clarity. (b) Overlay of the packing structures of **1** at 20 and −140 °C viewed along the *b* axis. The crystallographic *a* and *c* axes are indicated by arrows. The blue arrows indicate the shrinking direction of the packing structure along the *c* axis upon cooling.

Taking advantage of the mechanistic difference, the same crystal of **1** can exhibit sequential salient effects by cooling and then UV irradiation. When crystals of **1** were cooled from 20 to −150 °C, several crystals exhibited the thermosalient effect (Figure 7). For the second salient effect, keeping the temperature at −150 °C, the crystals were photoirradiated with UV light (365 nm). The crystals of **1** also exhibited the photosalient effect (Figure 7 and Movie S13). However, the photodimerized samples of **1** obtained after exhibiting the photosalient effect did not exhibit the thermosalient effect because photoirradiation produced **1**$_{PD}$, which does not exhibit the thermosalient effect. This is the first example of sequential salient effects of a single crystal based on two different mechanisms.

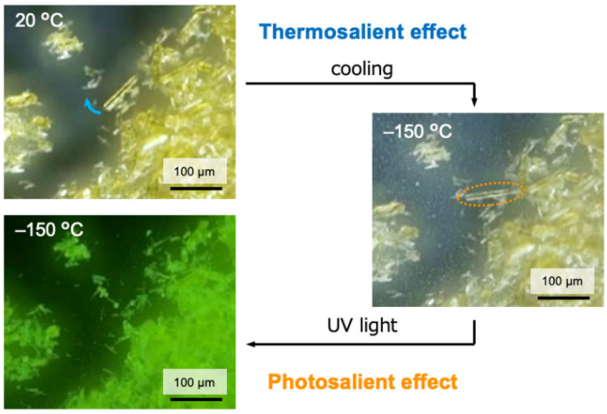


**Figure 7.** Photographs showing the sequential salient effects (thermosalient effect → photosalient effect) of the same crystalline sample of **1** by cooling and then UV photoirradiation (365 nm). The blue arrow indicates the directions of the jumps as a result of the thermosalient effect. Orange ellipse indicates the crystal showing photosalient effect.

Similar to **1**, the structure changes of **2** and **3** caused by the salient effects were also investigated by XRD and DSC analyses. When UV light was irradiated on crystalline samples of **2** and **3**, their photodimers ($\mathbf{2}_{PD}$ and $\mathbf{3}_{PD}$) formed, which were detected by $^1$H NMR and HRMS (Figures S18 and S19).[58] These photodimers indicated that the photosalient effect of **2** and **3** was also initiated by photodimerization of the anthracene moieties. Similar to **1**, DSC analysis of **2** and **3** gave featureless traces from –140 to 100 °C (Figure S20). These traces indicated that the thermosalient effect of **2** and **3** occurs without thermal phase transitions. Temperature-dependent XRD analysis of **3** upon cooling showed anisotropic lattice dimension changes ($\Delta a$ = –0.041 Å (–0.3%); $\Delta b$ = –0.225 Å (–1.5%); $\Delta c$ = –0.116 Å (–0.6%); 20 °C → –140 °C)) (Table S2 and Figures S21–S27).[59] These results suggest that the mechanisms of the salient effects of **2** and **3** are similar to those of **1**.

## CONCLUSION

In summary, we have reported aryl(9-isocyanoanthracene)gold(I) complexes (**1**, **2**, and **3**) exhibiting both the photosalient effect and thermosalient effect based on different mechanisms. Single-crystal XRD analysis, $^1$H NMR, and HRMS indicate that the photosalient effect of **1** is triggered by intermolecular photodimerization reaction of the anthracene moieties in the crystal. Temperature-dependent XRD analysis indicates that the thermosalient effect of **1** is caused by anisotropic thermal contraction upon cooling without a thermal phase transition. The mechanism difference of these salient effects enables sequential multisalient jumping of one crystal by UV irradiation and cooling. The mechanisms of the two salient effects of **2** and **3** were also investigated. These salient effects of single molecular crystals will provide a new guideline for designing multisalient crystals.

## ASSOCIATED CONTENT

**Supporting Information**.
Spectroscopic details; X-ray crystallographic details; thermal analyses; and other additional information; this material is available free of charge via the Internet at http://pubs.acs.org.

### Author Contributions

All authors have given approval to the final version of the manuscript.

## ACKNOWLEDGMENTS

This work was supported by a Grant-in-Aid for Japan Society for the Promotion of Science (JSPS) Fellows JP20J00103 and JSPS KAKENHI grants JP17H06370, JP19H02784, and JP19H04555. This work was also supported by the Institute for Chemical Reaction Design and Discovery (ICReDD), which was established by the World Premier International Research Initiative (WPI) of the Ministry of Education, Culture, Sports, Science and Technology (MEXT), Japan.

## REFERENCES

(1) For reviews on salient effects of organic and organometallic crystals, see: (a) Sahoo, S. C.; Panda, M. K.; Nath, N. K.; Naumov, P. Biomimetic Crystalline Actuators: Structure–Kinematic Aspects of the Self-Actuation and Motility of Thermosalient Crystals. *J. Am. Chem. Soc.* **2013**, *135*, 12241–12251. (b) Nath, N. K.; Panda, M. K.; Sahoo, S. C.; Naumov, P. Thermally Induced and Photoinduced Mechanical Effects in Molecular Single Crystals—A Revival. *CrystEngComm* **2014**, *16*, 1850–1858. (c) Naumov, P.; Chizhik, S.; Panda, M. K.; Nath, N. K.; Boldyreva, E. Mechanically Responsive Molecular Crystals. *Chem. Rev.* **2015**, *115*, 12440–12490. (d) Commins, P.; Desta, I. T.; Karothu, D. P.; Panda, M. K.; Naumov, P. Crystals on the Move: Mechanical Effects in Dynamic Solids. *Chem. Commun.* **2016**, *52*, 13941–13954. (e) Horie, M.; Wang, C.-H. Stimuli-Responsive Dynamic Pseudorotaxane Crystals. *Mater. Chem. Front.* **2019**, *3*, 2258–2269. (f) Karothu, D. P.; Halabi, J. M.; Li, L.; Colin-Molina, A.; Rodríguez-Molina, B.; Naumov, P. Global Performance Indices for Dynamic Crystals as Organic Thermal Actuators. *Adv. Mater.* **2020**, *32*, 1906216. (g) Naumov, P.; Karothu, D. P.; Ahmed, E.; Catalano, L.; Commins, P.; Halabi, J. M.; Al-Handawi, M. B.; Li, L. The Rise of the Dynamic Crystals. *J. Am. Chem. Soc.* **2020**, *142*, 13256–13272.

(2) (a) For the first report of salient effect, see: Etter, M. C.; Siedle, A. R. Solid-State Rearrangement of (Phenylazophenyl)palladium Hexafluoroacetylacetonate. *J. Am. Chem. Soc.* **1983**, *105*, 641–643. (b) For the first notation of "thermosalient" in a paper, see: Gigg, J.; Gigg, R.; Payne, S.; Conant, R. The Allyl Group for Protection in Carbohydrate Chemistry. Part 21. (±)-1,2:5.6- and (±)-1,2:3,4-Di-*O*-isopropylidene-*myo*-inositol. The Unusual Behaviour of Crystals of (±)-3,4-Di-*O*-acetyl-1,2,5,6-tetra-*O*-benzyl-*myo*-inositol on Heating and Cooling: A 'Thermosalient Solid'. *J. Chem. Soc., Perkin Trans. 1*, **1987**, 2411–2414.

(3) For photosalient effects by ring-opening/closing reactions, see: (a) Colombier, I.; Spagnoli, S.; Corval, A.; Baldeck, P. L.; Giraud, M.; Léaustic, A.; Yu, P. Strong Photomechanical Effects in Photochromic Organic Microcrystals. *Mol. Cryst. Liq. Cryst.* **2005**, *431*, 495–499. (b) Colombier, I.; Spagnoli, S.; Corval, A.; Baldeck, P. L.; Giraud, M.; Leaustic, A.; Yu, P.;

Irie, M. Diarylethene Microcrystals Make Directional Jumps upon Ultraviolet Irradiation. *J. Chem. Phys.* **2007**, *126*, 011101. (c) Kitagawa, D.; Okuyama, T.; Tanaka, R.; Kobatake, S. Photoinduced Rapid and Explosive Fragmentation of Diarylethene Crystals Having Urethane Bonding. *Chem. Mater.* **2016**, *28*, 4889–4892. (d) Hatano, E.; Morimoto, M.; Hyodo, K.; Yasuda, N.; Yokojima, S.; Nakamura, S.; Uchida, K. Photosalient Effect of a Diarylethene with a Perfluorocyclohexene Ring. *Chem. Eur. J.* **2016**, *22*, 12680–12683. (e) Hatano, E.; Morimoto, M.; Imai, T.; Hyodo, K.; Fujimoto, A.; Nishimura, R.; Sekine, A.; Yasuda, N.; Yokojima, S.; Nakamura, S.; Uchida, K. Photosalient Phenomena that Mimic Impatiens Are Observed in Hollow Crystals of Diarylethene with a Perfluorocyclohexene Ring. *Angew. Chem., Int. Ed.* **2017**, *56*, 12576–2580. (f) Nakagawa, Y.; Morimoto, M.; Yasuda, N.; Hyodo, K.; Yokojima, S.; Nakamura, S.; Uchida, K. Photosalient Effect of Diarylethene Crystals of Thiazoyl and Thienyl Derivatives. *Chem. Eur. J.* **2019**, *25*, 7874–7880.

(4) For photosalient effect by cycloadditions, see: (a) Naumov, P.; Kowalik, J.; Solntsev, K. M.; Baldridge, A.; Moon, J.-S.; Kranz, C.; Tolbert, L. M. Topochemistry and Photomechanical Effects in Crystals of Green Fluorescent Protein-Like Chromophores: Effects of Hydrogen Bonding and Crystal Packing. *J. Am. Chem. Soc.* **2010**, *132*, 5845–5857. (b) Kim, T.; Zhu, L.; Mueller, L. J.; Bardeen, C. J. Dependence of the Solid-State Photomechanical Response of 4-Chlorocinnamic Acid on Crystal Shape and Size. *CrystEngComm* **2012**, *14*, 7792–7799. (c) Medishetty, R.; Husain, A.; Bai, Z.; Runčevski, T.; Dinnebier, R. E.; Naumov, P.; Vittal, J. J. Single Crystals Popping Under UV Light: A Photosalient Effect Triggered by a [2+2] Cycloaddition Reaction. *Angew. Chem., Int. Ed.* **2014**, *53*, 5907–5911. (d) Medishetty, R.; Sahoo, S. C.; Mulijanto, C. E.; Naumov, P.; Vittal, J. J. Photosalient Behavior of Photoreactive Crystals. *Chem. Mater.* **2015**, *27*, 1821–1829. (e) Nath, N. K.; Runčevski, T.; Lai, C.-Y.; Chiesa, M.; Dinnebier, R. E.; Naumov, P. Surface and Bulk Effects in Photochemical Reactions and Photomechanical Effects in Dynamic Molecular Crystals. *J. Am. Chem. Soc.* **2015**, *137*, 13866–13875. (f) Mishra, M. K.; Mukherjee, A.; Ramamurty, U.; Desiraju, G. R. Crystal Chemistry and Photomechanical Behavior of 3,4-Dimethoxycinnamic Acid: Correlation Between Maximum Yield in the Solid-State Topochemical Reaction and Cooperative Molecular Motion. *IUCrJ* **2015**, *2*, 653–660. (g) Mulijanto, C. E.; Quah, H. S.; Tan, G. K.; Donnadieu, B.; Vittal, J. J. Curved Crystal Morphology, Photoreactivity and Photosalient Behaviour of Mononuclear Zn(II) Complexes. *IUCrJ* **2017**, *4*, 65–71. (h) Wang, H.; Chen, P.; Wu, Z.; Zhao, J.; Sun, J.; Lu, R. Bending, Curling, Rolling, and Salient Behavior of Molecular Crystals Driven by [2+2] Cycloaddition of a Styrylbenzoxazole Derivative. *Angew. Chem., Int. Ed.* **2017**, *56*, 9463–9467. (i) Yadava, K.; Vittal, J. J. Photosalient Behavior of Photoreactive Zn(II) Complexes. *Cryst. Growth Des.* **2019**, *19*, 2542–2547. (j) Dutta, B.; Sinha, C.; Mir, M. H. The Sunlight-Driven Photosalient Effect of a 1D Coordination Polymer and the Release of an Elusive Cyclobutane Derivative. *Chem. Commun.* **2019**, *55*, 11049–11051. (k) Mir, M. H.; Dutta, B.; Islam, S.; Khan, S. Solid-State Photodimerization via [2+2] Cycloaddition in Metal Complexes and CPs. *J. Indian Chem. Soc.* **2019**, *96*, 1297–1301. (l) Yadava, K.; Gallo, G.; Bette, S.; Mulijanto, C. E.; Karothu, D. P.; Park, I.-H.; Medishetty, R.; Naumov, P.; Dinnebier, R. E.; Vittal, J. J. Extraordinary Anisotropic Thermal Expansion in Photosalient Crystals. *IUCrJ* **2020**, *7*, 83–89. (m) Tong, F.; Xu, W.; Guo, T.; Lui, B. F.; Hayward, R. C.; Palffy-Muhoray, P.; Al-Kaysi, R. O.; Bardeen. C. J. Photomechanical Molecular Crystals and Nanowire Assemblies Based on the [2+2] Photodimerization of a Phenylbutadiene Derivative. *J. Mater. Chem. C* **2020**, *8*, 5036–5044. (n) Rath, B. B; Vittal, J. J. Single-Crystal-to-Single-Crystal [2 + 2] Photocycloaddition Reaction in a Photosalient One-Dimensional Coordination Polymer of Pb(II). *J. Am. Chem. Soc.* **2020**, *142*, 20117–20123.

(5) For an example of photosalient effect by rearrangement, see: (a) Matsuura, T.; Sata, Y.; Ogra, K.; Mori, M. Photoinduced Reactions. XXIII. A Novel Photorearrangement of Santonin in the Solid State. *Tetrahedron Lett.* **1968**, *44*, 4627–4630. (b) Commins, P.; Natarajan, A.; Tsai, C.-K.; Khan, S. I.; Nath, N. K.; Naumov, P.; Garcia-Garibay, M. A. Structure–Reactivity Correlations and Mechanistic Understanding of the Photorearrangement and Photosalient Effect of α-Santonin and Its Derivatives in Solutions, Crystals, and Nanocrystalline Suspensions. *Cryst. Growth Des.* **2015**, *15*, 1983–1990.

(6) For an example of photosalient effect by linkage isomerization, see: (a) Naumov, P.; Sahoo, S. C.; Zakharov, B. A.; Boldyreva, E. V. Dynamic Single Crystals: Kinematic Analysis of Photoinduced Crystal Jumping (The Photosalient Effect). *Angew. Chem., Int. Ed.* **2013**, *52*, 9990–9995. (b) Muya, J. T.; Meher, B. R.; Sahoo, S. C.; Chung, H. A Theoretical Insight into the Role of Counter Anions and Their Interactions in Nitropentaamminecobalt(III) Toward Linkage Isomerism-Induced Photochemical Motion. *Int. J. Quantum Chem.* **2019**, *119*, e25929.

(7) For photosalient effects without photochemical covalent/coordination bond formation, see: (a) Seki, T.; Sakurada, K.; Muromoto, M.; Ito, H. Photoinduced Single-Crystal-to-Single-Crystal Phase Transition and Photosalient Effect of a Gold(I) Isocyanide Complex with Shortening of Intermolecular Aurophilic Bonds. *Chem. Sci.* **2015**, *6*, 1491–1497. (b) Gupta, P.; Panda, T.; Allu, S.; Borah, S.; Baishya, A.; Gunnam, A.; Nangia, A.; Naumov, P.; Nath, N. K. Crystalline Acylhydrazone Photoswitches with Multiple Mechanical Responses. *Cryst. Growth Des.* **2019**, *19*, 3039–3044.

(8) (a) Etter, M. C.; Siedle, A. R. Crystal Expansion During a Thermochromic Transformation. *Mol. Cryst. Liq. Cryst.* **1983**, *96*, 35–38. (b) Panda, M. K.; Runčevski, T.; Sahoo, S. C.; Belik, A. A.; Nath, N. K.; Dinnebier, R. E.; Naumov, P. Colossal Positive and Negative Thermal Expansion and Thermosalient Effect in a Pentamorphic Organometallic Martensite. *Nat. Commun.* **2014**, *5*, 4811. (c) Khalil, A.; Karothu, D. P.; Naumov, P. Direct Quantification of Rapid and Efficient Single-Stroke Actuation by a Martensitic Transition in a Thermosalient Crystal. *J. Am. Chem. Soc.* **2019**, *141*, 3371–3375.

(9) Steiner, T.; Hinrichs, W.; Saenger, W.; Gigg, R. 'Jumping Crystals': X-ray Structures of the Three Crystalline Phases of (±)-3,4-Di-*O*-acetyl-1,2,5,6-tetra-*O*-benzyl-*myo*-inositol. *Acta Cryst.* **1993**, *B49*, 708–718.

(10) (a) Kohne, B.; Praefcke, K.; Mann, G. Perhydropyren, ein beim Phasenübergang Hüpfender Kohlenwasserstoff. *Chimia* **1988**, *42*, 139–141. (b) Ding, J.; Herbst, R.; Praefcke, K.; Kohne, B.; Saenger, W. A Crystal that Hops in Phase Transition, the Structure of *trans,trans,anti,trans,trans*-Perhydropyrene. *Acta Cryst.* **1991**, *B47*, 739–742.

(11) (a) Davey, R. J.; Maginn, S. J.; Andrews, S. J.; Black, S. N.; Buckley, A. M.; Cottier, D.; Dempsey, P.; Plowman, R.; Rout, J. E.; Stanley, D. R.; Taylor, A. Morphology and Polymorphism of Terephthalic Acid. *Mol. Cryst. Liq. Cryst.* **1994**, *242*, 79–90. (b) Karothu, D. P.; Weston, J.; Desta, I. T.; Naumov, P. Shape-Memory and Self-Healing Effects in Mechanosalient Molecular Crystals. *J. Am. Chem. Soc.* **2016**, *138*, 13298–13306.

(12) (a) Zamir, S.; Bernstein, J.; Greenwood, D. J. A Single Crystal to Single Crystal Reversible Phase Transition Which Exhibits the "Hopping Effect". *Mol. Cryst. Liq. Cryst.* **1994**, *242*, 193–200. (b) Skoko, Ž.; Zamir, S.; Naumov, P.; Bernstein, J. The Thermosalient Phenomenon. "Jumping Crystals" and Crystal Chemistry of the Anticholinergic Agent Oxitropium Bromide. *J. Am. Chem. Soc.* **2010**, *132*, 14191–14202.

(13) Corbett, J. M.; Dickman, M. H. 4,5-Bis(fluorodinitromethyl)-2-methoxy-1,3-dioxolane. *Acta Cryst.* **1996**, *C52*, 1851–1853.

(14) (a) Lieberman, H. F.; Davey, R. J.; Newsham, D. M. T. Br···Br and Br···H Interactions in Action: Polymorphism, Hopping, and Twinning in 1,2,4,5-Tetrabromobenzene. *Chem. Mater.* **2000**, *12*, 490–494. (b) Sahoo, S. C.; Sinha, S. B.; Kiran, M. S. R. N.; Ramamurty, U.; Dericioglu, A. F.; Reddy, C. M.; Naumov, P. Kinematic and Mechanical Profile of the Self-Actuation of Thermosalient Crystal Twins of 1,2,4,5-Tetrabromobenzene: A Molecular Crystalline Analogue of a Bimetallic Strip. *J. Am. Chem. Soc.* **2013**, *135*, 13843–13850. (c) Khalil, A.; Ahmed, E.; Naumov, P. Metal-Coated Thermosalient Crystals as Electrical Fuses. *Chem. Commun.* **2017**, *53*, 8470–8473. (d) Khalil, A.; Hu, C. T.; Naumov, P. Nanoscale Crystallization and Thermal Behaviour of 1,2,4,5-Tetrabromobenzene. *CrystEngComm* **2018**, *20*, 636–642. (e) Zakharov, B. A.; Michalchuk, A. A. L.; Morrison, C. A.; Boldyreva, E. V. Anisotropic Lattice Softening Near the Structural Phase Transition in the Thermosalient Crystal 1,2,4,5-Tetrabromobenzene. *Phys. Chem. Chem. Phys.* **2018**, *20*, 8523–8532. (f) Zaczek, A. J.; Catalano, L.; Naumov, P.; Korter, T. M. Mapping the Polymorphic Transformation Gateway Vibration in Crystalline 1,2,4,5-Tetrabromobenzene. *Chem. Sci.* **2019**, *10*, 1332–1341.

(15) Yasutake, M.; Sakamoto, Y.; Onaka, S.; Sako, K.; Tatemitsu, H.; Shinmyozu, T. Crystal Structural Properties of a Pinwheel Compound: [3$_6$](1,2,3,4,5,6)Cyclophane. *Tetrahedron Lett.* **2000**, *41*, 7933–7938.

(16) Siegrist, T.; Besnard, C.; Haas, S.; Schiltz, M.; Pattison, P.; Chernyshov, D.; Batlogg, B.; Kloc, C. A Polymorph Lost and Found: The High-Temperature Crystal Structure of Pentacene. *Adv. Mater.* **2007**, *19*, 2079–2082.

(17) (a) Wu, H.; Reeves-McLaren, N.; Pokorny, J.; Yarwood, J.; West, A. R. Polymorphism, Phase Transitions, and Thermal Stability of L-Pyroglutamic Acid. *Cryst. Growth Des.* **2010**, *10*, 3141–3148. (b) Panda, M. K.; Runčevski, T.; Husain, A.; Dinnebier, R. E.; Naumov, P. Perpetually Self-Propelling Chiral Single Crystals. *J. Am. Chem. Soc.* **2015**, *137*, 1895–1902. (c) Lončarić, I.; Popović, J.; Despoja, V.; Burazer, S.; Grgičević, I.; Popović, D.; Skoko, Ž. Reversible Thermosalient Effect of *N′*-2-Propylidene-4-hydroxybenzohydrazide Accompanied by an Immense Negative Compressibility: Structural and Theoretical Arguments Aiming Toward the Elucidation of Jumping Phenomenon. *Cryst. Growth Des.* **2017**, *17*, 4445–4453.

(18) (a) Centore, R.; Jazbinsek, M.; Tuzi, A.; Roviello, A.; Capobianco, A.; Peluso, A. A Series of Compounds Forming Polar Crystals and Showing Single-Crystal-to-Single-Crystal Transitions Between Polar Phases. *CrystEngComm* **2012**, *14*, 2645–2653. (b) Panda, M. K.; Centore, R.; Causà, M.; Tuzi, A.; Borbone. F.; Naumov, P. Strong and Anomalous Thermal Expansion Precedes the Thermosalient Effect in Dynamic Molecular Crystals. *Sci. Rep.* **2016**, *6*, 29610.

(19) (a) Lusi, M.; Bernstein, J. On the Propulsion Mechanism of "Jumping" Crystals. *Chem. Commun.* **2013**, *49*, 9293–9295. (b) Nauha, E.; Naumov, P.; Lusi, M. Fine-Tuning of a Thermosalient Phase Transition by Solid Solutions. *CrystEngComm* **2016**, *18*, 4699–4703.

(20) Ghosh, S.; Mishra, M. K.; Ganguly, S.; Desiraju, G. R. Dual Stress and Thermally Driven Mechanical Properties of the Same Organic Crystal: 2,6-Dichlorobenzylidene-4-fluoro-3-nitroaniline. *J. Am. Chem. Soc.* **2015**, *137*, 9912–9921.

(21) Engel, E. R.; Smith, V. J.; Bezuidenhout, C. X.; Barbour, L. J. Thermoresponsive Organic Inclusion Compounds: Modification of Thermal Expansion Behavior by Simple Guest Replacement. *Chem. Mater.* **2016**, *28*, 5073–5079.

(22) (a) Vicente, A. I.; Joseph, A.; Ferreira, L. P.; Carvalho, M. D.; Rodrigues, V. H. N.; Duttine, M.; Diogo, H. P.; Minas da Piedade, M. E.; Calhorda, M. J.; Martinho, P. N. Dynamic Spin Interchange in a Tridentate Fe(III) Schiff-Base Compound. *Chem. Sci.* **2016**, *7*, 4251–4258. (b) Martins, F. F.; Joseph, A.; Diogo, H. P.; Minas da Piedade, M. E.; Ferreira, L. P.; Carvalho, M. D.; Barroso, S.; Romão, M. J.; Calhorda, M. J.; Martinho, P. N. Irreversible Magnetic Behaviour Caused by the Thermosalient Phenomenon in an Iron(III) Spin Crossover Complex. *Eur. J. Inorg. Chem.* **2018**, *25*, 2976–2983.

(23) Takeda, T.; Akutagawa, T. Anisotropic Dissociation of π–π Stacking and Flipping-Motion-Induced Crystal Jumping in Alkylacridones and Their Dicyanomethylene Derivatives. *Chem. Eur. J.* **2016**, *22*, 7763–7770.

(24) (a) Mittapalli, S.; Perumalla, D. S.; Nangia, A. Mechanochemical Synthesis of *N*-Salicylideneaniline: Thermosalient Effect of Polymorphic Crystals. *IUCrJ* **2017**, *4*, 243–250. (b) Werny, M. J.; Vittal, J. J. Regulating Thermosalient Behaviour in Three Polymorphs. *IUCrJ* **2017**, *4*, 202–203.

(25) Shibuya, Y.; Itoh, Y.; Aida, T. Jumping Crystals of Pyrene Tweezers: Crystal-to-Crystal Transition Involving π/π-to-CH/π Assembly Mode Switching. *Chem. Asian J.* **2017**, *12*, 811–815.

(26) Ohtani, S.; Gon, M.; Tanaka, K.; Chujo, Y. A Flexible, Fused, Azomethine–Boron Complex: Thermochromic Luminescence and Thermosalient Behavior in Structural Transitions between Crystalline Polymorphs. *Chem. Eur. J.* **2017**, *23*, 11827–11833.

(27) Mittapalli, S.; Perumalla, D. S.; Nanuboluc, J. B.; Nangia, A. Thermomechanical Effect in Molecular Crystals: The Role of Halogen-Bonding Interactions. *IUCrJ* **2017**, *4*, 812–823.

(28) Tamboli, M. I.; Karothu, D. P.; Shashidhar, M. S.; Gonnade, R. G.; Naumov, P. Effect of Crystal Packing on the Thermosalient Effect of the Pincer-Type Diester Naphthalene-2,3-diyl-bis(4-fluorobenzoate): A New Class II Thermosalient Solid. *Chem. Eur. J.* **2018**, *24*, 4133–4139.

(29) Rawat, H.; Samanta, R.; Bhattacharya, B.; Deolka, S.; Dutta, A.; Dey, S.; Raju, K. B.; Reddy, C. M. Thermosalient Forms: Carryover of Thermosalient Behavior of Coformers from Single Component to Multicomponent Forms? *Cryst. Growth Des.* **2018**, *18*, 2918–2923.

(30) Raju, K. B.; Ranjan, S.; Vishnu, V. S.; Bhattacharya, M.; Bhattacharya, B.; Mukhopadhyay, A. K.; Reddy, C. M. Rationalizing Distinct Mechanical Properties of Three Polymorphs of a Drug Adduct by Nanoindentation and Energy Frameworks Analysis: Role of Slip Layer Topology and Weak Interactions. *Cryst. Growth Des.* **2018**, *18*, 3927–3937.

(31) Singh, M.; Chopra, D. Diversity in Mechanical Response in Donor–Acceptor Coupled Cocrystal Stoichiomorphs Based on Pyrene and 1,8-Dinitroanthraquinone Systems. *Cryst. Growth Des.* **2018**, *18*, 6670–6680.

(32) Alimi, L. O.; van Heerden, D. P.; Lama, P.; Smith, V. J.; Barbour, L. J. Reversible Thermosalience of 4-Aminobenzonitrile. *Chem. Commun.* **2018**, *54*, 6208–6211.

(33) Singh, M.; Bhandary, S.; Bhowal, R.; Chopra, D. Observation of Bending, Cracking and Jumping Phenomena on Cooling

and Heating of Tetrahydrate Berberine Chloride Crystals. *CrystEngComm* **2018**, *20*, 2253–2257.
(34) Dharmarwardana, M.; Arimilli, B. S.; Luzuriaga, M. A.; Kwon, S.; Lee, H.; Appuhamillage, G. A.; McCandless, G. T.; Smaldone, R. A.; Gassensmith, J. J. The Thermo-Responsive Behavior in Molecular Crystals of Naphthalene Diimides and Their 3D Printed Thermochromic Composites. *CrystEngComm* **2018**, *20*, 6054–6060.
(35) So, H.-S.; Minami, T.; Jindo, T.; Matsumoto, S. Thermosalient Effect of Two Polymorphs of a Diketopyrrolopyrrole Dye with Different Crystal Systems and Molecular Arrangements. *CrystEngComm* **2018**, *20*, 5317–5320.
(36) Colin-Molina, A.; Karothu, D. P.; Jellen, M. J.; Toscano, R. A.; Garcia-Garibay, M. A.; Naumov, P.; Rodríguez-Molina, B. Thermosalient Amphidynamic Molecular Machines: Motion at the Molecular and Macroscopic Scales. *Matter.* **2019**, *1*, 1033–1046.
(37) Takeda, T.; Ozawa, M.; Akutagawa, T. Jumping Crystal of a Hydrogen-Bonded Organic Framework Induced by the Collective Molecular Motion of a Twisted π System. *Angew. Chem., Int. Ed.* **2019**, *58*, 10345–10352.
(38) Seki, T.; Mashimo, T.; Ito, H. Anisotropic Strain Release in a Thermosalient Crystal: Correlation between the Microscopic Orientation of Molecular Rearrangements and the Macroscopic Mechanical Motion. *Chem. Sci.* **2019**, *10*, 4185–4191.
(39) Gaztañaga, P.; Baggio, R.; Halac, E.; Vega, D. R. Thermal, Spectroscopic and Structural Analysis of a Thermosalient Phase Transformation in Tapentadol Hydrochloride. *Acta Cryst.* **2019**, *B75*, 183–191.
(40) Jin, J.; Wu, S.; Ma, Y.; Dong, C.; Wang, W.; Liu, X.; Xu, H.; Long, G.; Zhang, M.; Zhang, J.; Huang, W. Nucleation Control-Triggering Cocrystal Polymorphism of Charge-Transfer Complexes Differing in Physical and Electronic Properties. *ACS Appl. Mater. Interfaces* **2020**, *12*, 19718–19726.
(41) Omoto, K.; Nakae, T.; Nishio, M.; Yamanoi, Y.; Kasai, H.; Nishibori, E.; Mashimo, T.; Seki, T.; Ito, H.; Nakamura, K.; Kobayashi, N.; Nakayama, N.; Goto, H.; Nishihara, H. Thermosalience in Macrocycle-Based Soft Crystals via Anisotropic Deformation of Disilanyl Architecture. *J. Am. Chem. Soc.* **2020**, *142*, 12651–12657.
(42) Smets, M. M. H.; Kalkman, E.; Krieger, A.; Tinnemans, P.; Meekes, H.; Vlieg, E.; Cuppen, H. M. On the Mechanism of Solid-State Phase Transitions in Molecular Crystals – The Role of Cooperative Motion in (Quasi)racemic Linear Amino Acids. *IUCrJ* **2020**, *7*, 331–341.
(43) For thermosalient effects without thermal phase transitions, see: (a) Klaser, T.; Popović, J.; Fernandes, J. A.; Tarantino, C. S.; Zema, M.; Skoko, Ž. Does Thermosalient Effect Have to Concur with a Polymorphic Phase Transition? The Case of Methscopolamine Bromide. *Crystals* **2018**, *8*, 301. (b) Jin, M.; Yamamoto, S.; Seki, T.; Ito, H.; Garcia-Garibay, M. A. Anisotropic Thermal Expansion as the Source of Macroscopic and Molecular Scale Motion in Phosphorescent Amphidynamic Crystals. *Angew. Chem., Int. Ed.* **2019**, *58*, 18003–18010. (c) Seki, T.; Mashimo, T.; Ito, H. Crystal Jumping of Simple Hydrocarbons: Cooling-Induced Salient Effect of Bis-, Tri-, and Tetraphenylethene through Anisotropic Lattice Dimension Changes without Thermal Phase Transitions. *Chem. Lett.* **2020**, *49*, 174–177.
(44) Sahoo, S. C.; Nath, N. K.; Zhang, L.; Semreen, M. H.; Al-Tel, T. H.; Naumov, P. Actuation Based on Thermo/Photosalient Effect: A Biogenic Smart Hybrid Driven by Light and Heat. *RSC Adv.* **2014**, *4*, 7640–7647.
(45) Ahmed, E.; Karothu, D. P.; Warren, M.; Naumov, P. Shape-Memory Effects in Molecular Crystals. *Nat. Commun.* **2019**, *10*, 3723.
(46) Seki, T.; Sakurada, K.; Ito, H. Controlling Mechano- and Seeding-Triggered Single-Crystal-to-Single-Crystal Phase Transition: Molecular Domino with a Disconnection of Aurophilic Bonds. *Angew. Chem., Int. Ed.* **2013**, *52*, 12828–12832.
(47) The parallel displacement was calculated from a focused π–π plane distances and the distance between the centroid of the anthryl moiety and the centroid of a six-membered ring within the naphthyl group. See Figure S9 for more details.
(48) Becker, H.-D. Unimolecular Photochemistry of Anthracenes. *Chem. Rev.* **1993**, *93*, 145–172.
(49) Schmidt, G. M. J. Photodimerization in the Solid State. *Pure Appl. Chem.* **1971**, *27*, 647–678.
(50) The structure of **1**$_{PD}$ was also confirmed by $^1$H NMR spectroscopy and HRMS. In the $^1$H NMR spectra, the singlet peak of the proton at the 10-position of the anthracene ring of **1** at 8.72 ppm shifted to 4.95 ppm upon photodimerization (Figure S11). Moreover, electrospray ionization mass spectrometry also detected the molecular weight of **1**$_{PD}$. ESI-MS (*m*/*z*): $[M+Na]^+$ calcd. for $C_{50}H_{32}Au_2N_2Na$, 1077.17942; found, 1077.17618.
(51) Photodimers of anthracene often revert to monomers by photochemical or thermal dissociation. For example, see ref 52. However, we could not confirm thermal dissociation of the photodimers (**1**$_{PD}$, **2**$_{PD}$, and **3**$_{PD}$), possibly because these photodimers were thermally unstable under high-temperature conditions (i.e., above 150 °C). In addition, we could not confirm photochemical dissociation.
(52) Bouas-Laurent, H.; Castellan, A.; Desvergne, J.-P.; Lapouyade, R. Photodimerization of Anthracenes in Fluid Solutions: (Part 2) Mechanistic Aspects of the Photocycloaddition and of the Photochemical and Thermal Cleavage. *Chem. Soc. Rev.* **2001**, *30*, 248–263.
(53) The Au(I)···Au(I) distance of the **1**$_{PD}$ crystal (3.463(1) Å) is shorter than that of the **1** crystal (3.6714(5) Å). With the change of hybridization of the connecting carbon atoms from $sp^2$ to $sp^3$ by photodimerization, the isocyanide moieties are distorted from the anthracene plane. As a result, the Au(I) atoms are pressed against each other in the **1**$_{PD}$ crystal (Figure S12).
(54) The number of molecules in the unit cell (*Z* value) of the **1**$_{PD}$ crystal is half that of the **1** crystal (**1**, $Z = 4$; **1**$_{PD}$, $Z = 2$). However, the molecular formula of **1**$_{PD}$ is twice as that of **1** (**1**, $C_{25}H_{16}AuN$; **1**$_{PD}$, $C_{50}H_{32}Au_2N_2$). This means that the numbers of atoms in the unit cells are equal. Therefore, the change of the volume before and after photodimerization is represented by the change of the unit cell volume.
(55) Using the crystallographic parameters at different temperatures, PASCal software visualized the anisotropic lattice dimension change of **1** upon cooling. A plot of the expansivity indicatrices of **1** is shown in Figure S14. The contraction of the crystal upon cooling primarily occurs along the *c* axis with a thermal expansion coefficient of 97.9 $MK^{-1}$. For PASCal software, see ref 56.
(56) Cliffe, M. J.; Goodwin, A. L. PASCal: A Principal Axis Strain Calculator for Thermal Expansion and Compressibility Determination. *J. Appl. Cryst.* **2012**, *45*, 1321–329.
(57) Simulated powder diffraction patterns derived from the single-crystal structures of **1** are fairly changed (Figure S15), supporting the absence of the thermal phase transitions.
(58) The crystal qualities of the photodimers (**2**$_{PD}$ and **3**$_{PD}$) were not satisfactory for single-crystal XRD because these monomer crystals are broken down into fine crystals after photodimerization. However, the structure of **2**$_{PD}$ and **3**$_{PD}$

were confirmed by $^1$H NMR spectroscopy and HRMS. See Figures S18 and S19.

(59) Because of the high reactivity of **2** for photodimerization even under ambient light, we could not obtain a single crystal of **2** suitable for XRD analysis.

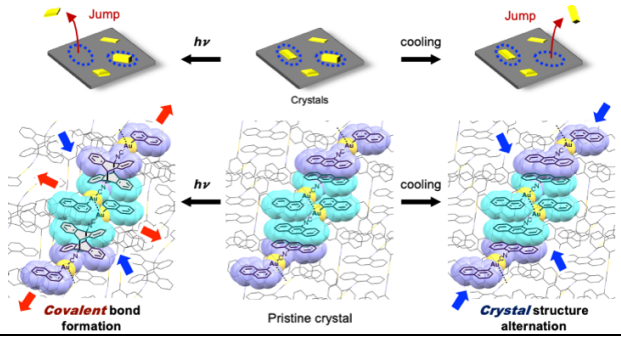
Jump
hν
Crystals
cooling
Jump
hν
cooling
Covalent bond formation
Pristine crystal
Crystal structure alternation